Tetracene air-gap single-crystal field-effect transistors

Yu Xia, Vivek Kalihari, and C. Daniel Frisbie[a)]
Department of Chemical Engineering and Materials Science, University of Minnesota, 421 Washington Avenue SE, Minneapolis, Minnesota 55455

Nam K. Oh and John A. Rogers
Frederick Seitz Materials Research Laboratory, Department of Materials Science and Engineering, University of Illinois at Urbana-Champaign, Urbana, Illinois 61801

(Received 20 February 2007; accepted 15 March 2007; published online 17 April 2007)

The authors report the fabrication and characterization of tetracene single-crystal field-effect transistors (FETs) utilizing an air or vacuum gap as the gate dielectric. The linear mobility of the device can be as high as 1.6 $cm^2/V\,s$ in air, with a subthreshold slope lower than 0.5 V nF/decade cm^2. By changing the orientation of the same crystal on the air-gap substrate, surface charge transport along different crystallographic directions was measured. There is pronounced anisotropy in the mobility; temperature dependent measurements show the mobility is activated (in contrast to air-gap FETs based on rubrene) and that the activation energy is independent of transport direction. Gate electrode displacement current was also recorded for these devices, allowing accurate determination of the gate induced surface charge and the fraction of trapped charge. © *2007 American Institute of Physics*. [DOI: 10.1063/1.2724895]

Recently, there has been significant progress in understanding the physics of carrier transport in field-effect transistors (FETs) based on single crystals of the organic semiconductor rubrene.[1–9] In principle, single-crystal organic FETs (SC-OFETs) offer some clear advantages relative to organic thin film transistors for transport studies because of the absence of complex microstructure.[10,11] Yet, even the surface of single crystals can be less than ideal for transport studies because of the presence of defects, for example, step edges and line dislocations. The exciting results on rubrene motivate similar investigations on other single-crystal organic semiconductors, with the long term goal of elucidating the role of molecular structure and crystal packing on electrical transport.

In this letter, we focus on tetracene based SC-OFETs employing an air or vacuum gap as the gate dielectric, as sketched in Fig. 1(a). This air-gap device structure is similar to that used for rubrene SC-OFETs as described by Menard *et al.*[2] The air gap provides a pristine interface between crystal and gate dielectric, which reduces the interface defects and minimizes the Fröhlich polaron effect.[12] In addition, crystals can be removed from the stamp and relaminated at different orientations so that the role of crystal anisotropy on transport can be investigated. Here we show that the transport behavior of tetracene air-gap SC-OFETs is qualitatively different from devices based on rubrene single crystals. Foremost, the room temperature mobility (1.6 $cm^2/V\,s$) is an order of magnitude lower and it is activated, whereas in rubrene air-gap SC-OFETs the mobility shows metallic behavior (i.e., it increases as temperature decreases).[4] Like rubrene transistors, however, the mobility in tetracene air-gap SC-OFETs is anisotropic with respect to crystallographic transport direction. We also demonstrate that displacement currents can be measured in these devices, which allows direct determination of injected and trapped charge densities in the channel.

Tetracene powder (98% purity) was purchased from Sigma-Aldrich and crystallized by means of horizontal physical vapor transport,[13] under a mixture of $Ar:H_2$ (~50:50 by volume) as the carrier gas. The gas velocity was approximately 1 mm/s. To increase the quality of final product, the obtained crystals were used as the source material for a subsequent growth and this procedure was repeated twice.

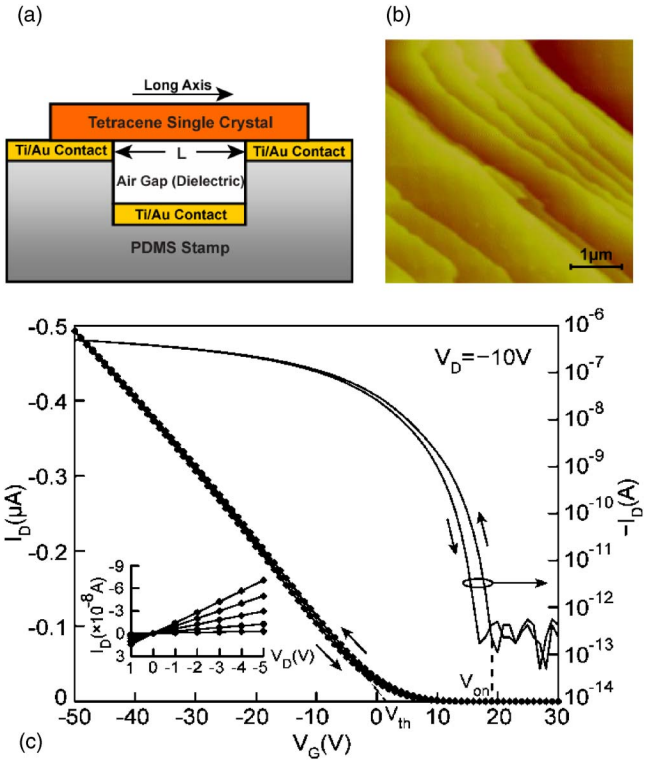

FIG. 1. (Color online) Tetracene air-gap SC-OFET. (a) Sketch of the device cross section. (b) AFM image for the surface of tetracene crystal. Steps can be clearly observed with 12±1 Å in height. (c) Transfer characteristic of the best device in air (sweep rate of 2.5 V/s). The linear mobility is 1.6 $cm^2/V\,s$ and the intrinsic swing is 0.3 V nF/decade cm^2. The inset in (c) shows the typical output characteristic of our devices in linear regime.

a)Electronic mail: frisbie@cems.umn.edu

The carrier gas was also purified by passing it over finely divided nickel (Aeronex model No. SS-400KGC-H-4S). Each growth process takes about a week and yields platelike crystals up to 100 μm in thickness. For the device studied in this letter, we always chose narrow plate-shaped tetracene crystals, approximately 5–10 mm in length and 0.4–1 mm in width. The crystals were characterized by atomic force microscopy (AFM, Veeco Metrology Nanoscope IIIa) and x-ray diffraction (Bruker-AXS microdiffractometer).

Field-effect transistors were fabricated by placing the long axis of a single crystal along the transistor channel as sketched in Fig. 1(a). A poly(dimethylsiloxane) (PDMS) stamp with a thin layer of Ti/Au (20/170 Å) coated on top was used as the substrate. The air gap served as the gate dielectric layer, and the metal-coated features functioned as source, drain, and gate electrodes, respectively. The channel length L varied from 100 to 200 μm, the dielectric thickness t was 4.9 μm measured by profilometry, and the width of source/drain electrodes was 1000 μm. However, in many cases, the real transistor channel width W was determined by the width of the crystal itself. Electrical characterization of the devices was performed using a standard probe station with Keithley 237 and 6517A electrometers.

Figure 1(c) shows the output characteristic of the best device in air. The linear mobility is 1.6 $cm^2/V\,s$, three times higher than the highest value reported on SiO_2 gate dielectric.[14] The device has a current on/off ratio I_{on}/I_{off} of 10^7, has a subthreshold slope of 0.3 V nF/decade cm^2, and shows relatively small hysteresis considering the 1 min long sweep cycle. Under vacuum ($<10^{-6}$ Torr), the transistor showed negligible change in performance compared to that in air. The aspect ratio (W/L) of this device was about 3.3. This aspect ratio is limited by the width of this crystal, which eliminates the possibility of fringe current. The inset in Fig. 1(c) shows the typical output characteristics. A linear (Ohmic) current voltage relationship can be observed when the bias along the channel V_{SD} is low, indicating relatively small resistance associated with the source/drain contacts. More than 15 devices were measured using tetracene single crystals from three different crystal growth batches. All FETs were fabricated with the long axis of the crystal aligned along the channel. In general, the linear mobility was within the range of 0.4–1.6 $cm^2/V\,s$, with subthreshold slope less than 0.5 V nF/decade cm^2. We noticed that the mobility tended to be smaller for thicker crystals. However, only thick crystals (50–100 μm in thickness) proved to be rigid enough to survive several relaminations during anisotropy studies.

Imaging by AFM revealed widely distributed steps on the surface of tetracene crystals. A typical topography image is shown in Fig. 1(b). The step heights (12±1 Å) are approximately one molecular layer thick ($\mathbf{c}^*$=12.3 Å for tetracene lattice). The average step density was found to be 1.4 step/μm, with certain regions where stacking of eight to ten steps occur [see the center part of Fig. 1(b) for example]. Similar steps have been reported on rubrene single crystals,[8] but with somewhat smaller step density and more uniform distribution. These defects can act as barriers and traps for surface charge transfer,[15] which will impair FET performance. Further work is needed to quantitatively assess the influence of steps on charge transport.

Figure 2(b) presents the transfer characteristics of four devices, fabricated by relaminating the same crystal over the PDMS gap along four different directions. The aspect ratio

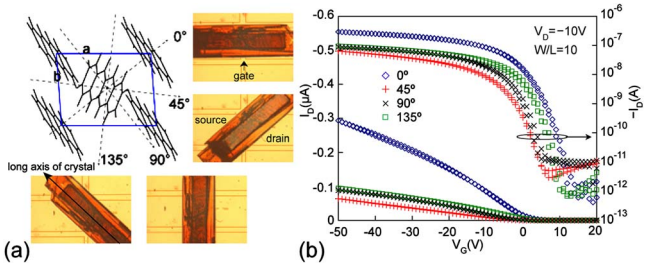

FIG. 2. (Color online) Anisotropic transistor properties. (a) Optical images of the devices with tetracene crystal relaminated at different angles along the channel and the associated crystal orientations for charge transfer. The surface of tetracene single crystal is parallel to the **a**-**b** basal plane of the crystal lattice, and the long axis coincides with the $[1\bar{1}0]$ orientation. (b) Transfer characteristic along different directions.

(W/L) is 10 for every device. The operation parameters and calculated quantities are tabulated in Table I. Threshold voltage V_{th} and turn on voltage V_{on} are defined in Fig. 1(c). The crystallographic orientation was obtained by comparing the angle between all the native boundaries on the crystal surface, and was confirmed with microdiffraction. The surface of each crystal corresponded to the **a**-**b** basal plane of the crystal lattice (this was also proved by AFM from the step height value); the long axis of the crystal corresponded to the $[1\bar{1}0]$ direction. In Fig. 2(a), we relate the crystal laminating directions with real orientations. Overall, we found that the field-effect mobility was strongly correlated with crystal orientation, with the highest mobility direction along $[1\bar{1}0]$. This observation fits well with theoretical predictions,[16] which indicate that the transfer integrals along the tetracene unit cell diagonal are the largest.

We then measured the device performance for the same crystal along two orientations in the temperature range of 200–310 K. For each direction, repeatable output characteristics were observed during the temperature ramp. The linear mobility at each temperature set point was calculated and plotted in Fig. 3(a). On cooling, the mobility decreased significantly with temperature, demonstrating clear Arrhenius behavior below 275 K. The mobility began to saturate above 300 K. We also studied similar devices with a four-probe configuration[17] to make sure that the activation behavior did not arise from contact effects. As shown in Fig. 3(a), the anisotropic behavior in mobility was also obtained for all temperatures. Furthermore, the temperature variance was identical. The activation energy E_a of charge transfer can be calculated from $\mu \approx \mu_0 \exp(-E_a/kT)$,[15] and it depends on gate voltage as demonstrated in the inset in Fig. 3(a). The gate voltage was corrected by the turn on voltage V_{on} for each direction to normalize the charge density. Interestingly, the activation energies along two directions decrease with increasing gate voltage and merge into the same trend line,

TABLE I. Parameters of tetracene SC-OFET at different transport angles.

Angle (deg)	μ_{max} ($cm^2/V\,s$)	V_{th} (V)	V_{on} (V)	S_i (V nF/decade cm^2)
0	0.4	7	14	0.5
45	0.07	2	6	0.5
90	0.1	7	12	0.4
135	0.1	3	6	0.6

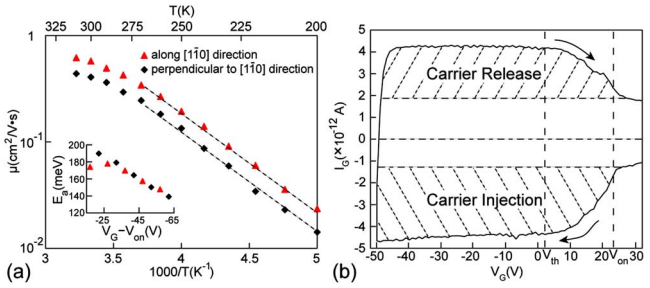

FIG. 3. (Color online) (a) Field-effect mobility vs temperature for devices with the same crystal laminated at two different directions. The inset shows the activation energies extrapolated at different gate voltages for two directions merge into the same trend line. (b) Displacement current measurement (sweep rate of 2.5 V/s) for a typical device. The injected carrier density is 8.1×10^{10} cm^{-2}; over 25% of these carriers were trapped after one sweep cycle.

indicating similar density of state distributions for surface traps. We also found this similarity in the activation energy of pentacene SC-OFETs when the crystal was laminated along two perpendicular directions. Such behavior was also reported previously on rubrene based air-gap SC-OFETs, although in a small temperature range (120–150 K).[4] In contrast, in an early time-of-flight experiment on naphthalene bulk single crystal at low temperature (<270 K), the activation energy was found to depend on transport directions.[18] The source of this directional independence in activation energy for surface charge transport requires further investigation.

Even at high gate voltage, the activation energy for the mobility is approximately 140 meV, which is much higher than that previously reported for tetracene SC-OFETs with SiO_2 gate dielectric.[14,17] This is probably due to the relatively small gate induced carrier density caused by the low capacitance of the air dielectric layer. Smaller carrier density means that not all of the deep traps (>100 meV) are filled. To quantify the injected charge density, we performed gate displacement current measurements[19] on the air-gap transistors. Figure 3(b) shows the displacement current for a typical device. The gate voltage was swept from +40 to −50 V, and then swept back to +40 V at the rate of 2.5 V/s, similar to our standard transfer characteristic measurement, with the source/drain electrodes grounded. The corresponding V_{th} and V_{on} obtained from transfer characteristic are also marked in the figure. In general, the gate displacement current is a function of the insulator capacitance and the gate voltage sweep rate:

$$I_G = \frac{dQ}{dt} = C\frac{dV_G}{dt} + V_G\frac{dC}{dt} \approx C_i\frac{dV_G}{dt}. \quad (1)$$

The current jump at $V=V_{on}$ is due to the increase in capacitance C_i, which arises when carriers are swept into the channel.

The injected carrier density can be calculated by integrating the current increment over the whole forward sweep from V_{on} to $V_{max}=-50$ V. For this device, the induced carrier density is 8.1×10^{10} cm^{-2} (approximately one hole per 2500 unit cells). The released carrier density can be obtained similarly from the reverse sweep and has a value of 5.7×10^{10} cm^{-2}. As a result, the trapped carrier density for this sweep cycle (the difference between the injected and released charges) is 2.4×10^{10} cm^{-2}; i.e., more than 25% of the total injected carriers were trapped. Injected carrier density in this air-gap device is approximately two orders of magnitude smaller than the value for typical SC-OFETs with a SiO_2 gate dielectric.[9] This is consistent with the higher transport activation energy because the smaller charge density means that a larger faction of carriers will be immobilized in deep traps.

In conclusion, the mobility in single-crystal tetracene air-gap OFETs is thermally activated at room temperature, presumably due to defects, in contrast to rubrene devices which show metallic behavior of the mobility. The mobility is anisotropic and the fastest transport direction is along [1$\bar{1}$0], the unit cell diagonal. Displacement current measurements can quantify the injected charge density and provide an opportunity to quantify trapped charge. Further work is needed to identify the physical and/or chemical nature of the traps and to understand the difference between rubrene and tetracene air-gap SC-OFETs.

The authors thank Etienne Menard, Bryan Olmsted, and Yan Liang for helpful discussion. This work was partially supported by the NSF Materials Research Science and Engineering Center Program (DMR-0212302). Support also came from the US Department of Energy, Office of Basic Energy Sciences.

[1] V. C. Sundar, J. Zaumseil, V. Podzorov, E. Menard, R. L. Willett, T. Someya, M. E. Gershenson, and J. A. Rogers, Science **303**, 1644 (2004).
[2] E. Menard, V. Podzorov, S.-H. Hur, A. Gaur, M. E. Gershenson, and J. A. Rogers, Adv. Mater. (Weinheim, Ger.) **16**, 2097 (2004).
[3] A. F. Stassen, R. W. I. de Boer, N. N. Iosad, and A. F. Morpurgo, Appl. Phys. Lett. **85**, 3899 (2004).
[4] V. Podzorov, E. Menard, A. Borissov, V. Kiryukhin, J. A. Rogers, and M. E. Gershenson, Phys. Rev. Lett. **93**, 086602 (2004).
[5] V. Podzorov, E. Menard, J. A. Rogers, and M. E. Gershenson, Phys. Rev. Lett. **95**, 226601 (2005).
[6] J. Takeya, K. Tsukagoshi, Y. Aoyagi, T. Takenobu, and Y. Iwasa, Jpn. J. Appl. Phys., Part 2 **44**, L1393 (2005).
[7] T. Takahashi, T. Takenobu, J. Takeya, and Y. Iwasa, Appl. Phys. Lett. **88**, 033505 (2006).
[8] E. Menard, A. Marchenko, V. Podzorov, M. E. Gershenson, D. Fichou, and J. A. Rogers, Adv. Mater. (Weinheim, Ger.) **18**, 1552 (2006).
[9] C. Goldmann, C. Krellner, K. P. Pernstich, S. Haas, D. J. Gundlach, and B. Batlogg, J. Appl. Phys. **99**, 034507 (2006).
[10] R. W. I. de Boer, M. E. Gershenson, A. F. Morpurgo, and V. Podzorov, Phys. Status Solidi A **201**, 1302 (2004).
[11] M. E. Gershenson, V. Podzorov, and A. F. Morpurgo, Rev. Mod. Phys. **78**, 973 (2006).
[12] I. N. Hulea, S. Fratini, H. Xie, C. L. Mulder, N. N. Iossad, G. Rastelli, S. Ciuchi, and A. F. Morpurgo, Nat. Mater. **5**, 982 (2006).
[13] R. A. Laudise, C. Kloc, P. G. Simpkins, and T. Siegrist, J. Cryst. Growth **187**, 449 (1998).
[14] R. W. I. de Boer, T. M. Klapwijk, and A. F. Morpurgo, Appl. Phys. Lett. **83**, 4345 (2003).
[15] M. Pope and C. E. Swenberg, *Electronic Processes in Organic Crystals and Polymers*, 2nd ed. (Oxford University Press, New York, 1999).
[16] D. A. da Silva Filho, E.-G. Kim, and J.-L. Bredas, Adv. Mater. (Weinheim, Ger.) **17**, 1072 (2005).
[17] C. R. Newman, R. J. Chesterfield, J. A. Merlo, and C. D. Frisbie, Appl. Phys. Lett. **85**, 422 (2004).
[18] J. Berrehar and M. Schott, Mol. Cryst. Liq. Cryst. **46**, 223 (1978).
[19] S. Ogawa, T. Naijo, Y. Kimura, H. Ishii, and M. Niwano, Synth. Met. **153**, 253 (2005).